Biomaterials 218 (2019) 119305

Contents lists available at ScienceDirect

Biomaterials

journal homepage: www.elsevier.com/locate/biomaterials

In vivo cancer targeting via glycopolyester nanoparticle mediated metabolic cell labeling followed by click reaction

Hua Wang[a,1], Yang Bo[a,1], Yang Liu[a], Ming Xu[a], Kaimin Cai[a], Ruibo Wang[a], Jianjun Cheng[a,b,*]

[a] Department of Materials Science and Engineering, United States
[b] Department of Bioengineering, University of Illinois at Urbana-Champaign, Urbana, IL, 61801, United States

ARTICLE INFO

Keywords:
Cancer targeting
Cell labeling
Click chemistry
Drug design
Sugar

ABSTRACT

We developed glycopolyesters (GPs) via azido-sugar initiated ring-opening polymerization of *O*-carboxyanhydrides (OCAs) and achieved efficient in vivo cancer targeting via GP-nanoparticle (GP-NP) mediated metabolic cell labeling followed by Click reaction. GP-NP shows controlled release of azido-sugars and can efficiently label LS174T colon cancer cells with azido groups in tumor-bearing mice. The exogenously introduced azido groups render excellent in vivo cancer targeting and retention of dibenzocyclooctyne-Cy5 (DBCO-Cy5) with an increasing tumor retention enhancement over time (68% at 6 h, 105% at 24 h, and 191% at 48 h) compared to control mice without azido labeling. The tumor accumulation of DBCO-doxorubicin is also significantly enhanced in GP-NP pretreated mice, resulting in improved in vivo anticancer efficacy. This study, for the first time, proposes the use of azido-sugar initiated polymerization of OCAs to form sugar delivery vehicles with high stability and controlled release, and demonstrates the increasing tumor targeting effect of DBCO-cargo over time by azido-modified tumor cells.

1. Introduction

Chemotherapy provides vital cancer treatment but often suffers from undesired pharmacological profiles of anticancer agents, such as poor water solubility, fast renal clearance, large volume of distribution, and severe side effects [1,2]. Drug loaded nanoparticle (NP) has emerged as a promising modality to solve these issues [3,4]. To further reduce side effects and improve anticancer efficacy, NP mediated cancer targeting has been attempted by modifying NP surface with targeting ligands (TLs) that can specifically bind to cancer-associated protein receptors [5–7]. Although these NP-TLs have improved uptake by cancer cells, they often show very limited targeting and undesired immune responses in vivo, the latter of which leads to the fast clearance of NP-TLs from circulation and their elevated accumulation in liver and spleen [8–12]. Alternative strategies to direct chemotherapeutic agents specifically to cancerous tissues with minimal effect on their distribution to other organs is clearly of great interest and importance for drug development and clinical oncology [13–16].

Click chemistry has been widely used in bioconjugation, cell labeling, and protein profiling because of their favorable features such as small ligand size, biocompatibility, high reaction rate, and excellent specificity [17–22]. The discovery that unnatural sugars (e.g., tetraacetyl *N*-azidoacetylmannosamine (Ac_4ManAz)) can metabolically label cancer cell surface with azido groups has enabled the application of Click chemistry to cancer targeting [23–29]. Differing from the targeting of the protein receptors by existing TLs which is mediated by hydrophobic/electrostatic interactions, the targeting of metabolically expressed azido-sugars is mediated by the formation of covalent bonds through efficient Click chemistry. Apart from the above-mentioned features of Click reaction, this sugar/Click chemistry mediated targeting strategy also avoids immune responses and benefits from the much larger number density of cell-surface sugars compared to proteins [30]. However, the metabolic labeling process of azido-sugars also occurs in healthy cells [25,31]. To enable the use of metabolic labeling followed by Click chemistry for cancer targeting, the key challenge is to either design azido-sugars with cancer-specific labeling capability or specifically deliver the azido-sugar to cancers [31–36].

Here we explore cancer targeting by integrating NP-mediated passive targeting via the Enhanced Permeability and Retention (EPR) effect [37–39] and azido-sugar mediated cancer cell labeling. We avoid the use of azido-sugar encapsulated NPs, as premature sugar release and uncontrolled release kinetics may make it difficult to achieve efficient cancer labeling [33,40]. An azido-sugar conjugated NP with great loading stability and controlled sugar release profiles can potentially

* Corresponding author. Department of Materials Science and Engineering, United States.
E-mail address: jianjunc@illinois.edu (J. Cheng).
[1] These authors contributed equally.

https://doi.org/10.1016/j.biomaterials.2019.119305
Received 5 March 2019; Received in revised form 21 June 2019; Accepted 24 June 2019
Available online 25 June 2019
0142-9612/ © 2019 Published by Elsevier Ltd.

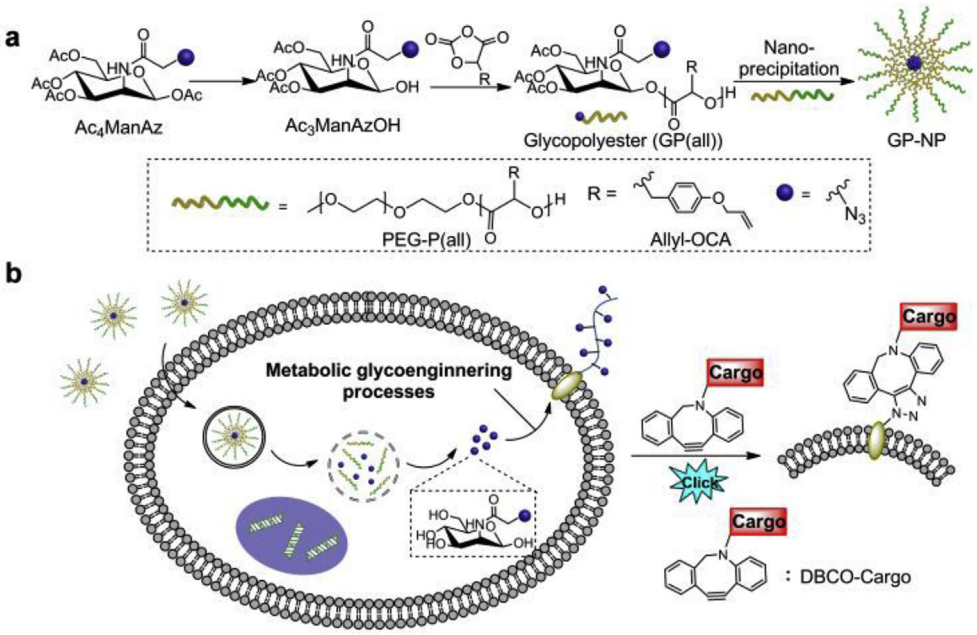

Scheme 1. Schematic illustration of the synthesis and metabolic labeling process of GP-NP. (a) Synthesis of glycopolyester (GP(all)) via Ac_3ManAzOH-initiated ROP of all-OCA, and preparation of GP-NP via nanoprecipitation method. (b) GP-NP mediated metabolic labeling of cancer cells with azido groups and subsequent targeting by DBCO-cargo via copper-free Click chemistry.

enable efficient cancer cell labeling and facilitate the subsequent Click chemistry-mediated cancer targeting. Specifically, we designed azido-sugar conjugated glycopolyester NP (GP-NP) via azido-sugar initiated ring-opening polymerization (ROP) of 5-(4-(prop-2-en-1-yloxy)benzyl)-1,3-dioxolane-2,4-dione (allyl (all)-OCA) followed by nanoprecipitation of the resulting GP(all) with PEG-P(all) (Scheme 1a). GP-NP showed excellent stability under physiological conditions while underwent controlled release of azido-sugars in the presence of cellular esterase for metabolic cell labeling (Scheme 1b). GP-NP mediated tumor labeling significantly improved tumor accumulation and retention of dibenzocyclooctyne (DBCO)-Cy5 and DBCO-doxorubicin conjugate.

2. Methods

2.1. General procedures for ring-opening polymerization of allyl-OCA

R-OH (1 molar equivalent) and 4-dimethylaminopyridine (1 molar equivalent) were dissolved in anhydrous DCM in a glove box, followed by the addition of allyl-OCA (20, 50, or 100 molar equivalents) in DCM in one portion. The reaction mixture was stirred at room temperature for 16 h. One drop of reaction solution was taken out for FTIR analysis to confirm the complete consumption of allyl-OCA (disappearance of the peak at around 1810 cm^{-1}). The mixture was then precipitated into diethyl ether. Collected precipitates were washed with anhydrous diethyl ether twice and dried for use.

2.2. Preparation of GP-NP and PP-NP

$GP(all)_{20}$ or $PP(all)_{20}$ (5 mg) and $mPEG_{5k}$-$P(all)_{20}$ (5 mg) were dissolved and well mixed in anhydrous DMF (1 mL). The mixture was then dropwise added to vigorously stirred nanopure water (20 mL). A turbid solution was obtained immediately. After addition of polymer solution, the mixture was stirred for another 2 h, and then transferred into a dialysis tube (MWCO 5k). The NPs were dialyzed against deionized water for 48 h, concentrated via ultracentrifugation, and stored for use.

2.3. Release kinetic study of GP-NP

(1) Conjugation of DBCO-Cy5 onto $GP(all)_{20}$: $GP(all)_{20}$ (5 mg, 1 molar equivalent of azido-sugar) and DBCO-Cy5 (100 μg, 0.1 molar equivalent) were dissolved in anhydrous methanol (1 mL), and the solution was stirred at room temperature for 2 h, at which time point HPLC showed the complete consumption of DBCO-Cy5. Potentially retained minimal amount of DBCO-Cy5 was removed via ultracentrifugation with a cut-off molecular weight of 2k. Collected polymers were dried and stored for use. (2) Preparation of Cy5-conjugated GP-NP: Cy5-labeled $GP(all)_{20}$ (5 mg) and $mPEG_{5k}$-$P(all)_{20}$ (5 mg) were dissolved, and well mixed in anhydrous DMF (1 mL). The mixture was then dropwise added to vigorously stirred nanopure water (20 mL). After addition of polymer solution, the mixture was stirred for another 2 h, and then transferred into a dialysis tube (MWCO 5k). The NPs were dialyzed against deionized water for 48 h, concentrated via ultracentrifugation, and stored for use. (3) Release study of Cy5-conjugated GP-NP: GP-NP was dispersed in PBS (10 mg/mL, 2 mL, pH 7.4) and transferred into a dialysis tube in the presence or absence of esterase (100 units). The dialysis tube was immersed in 30 mL of PBS (pH 7.4) and incubated at 37 °C (100 rpm). 1 mL of the medium was taken out for fluorescence measurement and the same amount of fresh medium was added at selected time points. Released sugar moieties were quantified by the standard curve of fluorescence intensity of Cy5.

2.4. Stability of NPs in 50% human serum

GP-NP or PP-NP in DI water (1 mg/mL, 100 μL) was diluted with human serum/PBS (1/1, v/v, 3 mL). Size and size distribution of NPs were monitored via DLS at selected time points.

2.5. In vitro cell labeling experiment

LS174T colon cancer cells were seeded onto coverslips in a 6-well plate with a cell density of 40 k/well. GP-NP (25 μM in GP equivalent) or PP-NP (25 μM in PP equivalent) was added and the cells were incubated at 37 °C for 72 h. The medium was removed and washed with PBS for three times. DBCO-Cy5 (25 μM) in Opti-MEM was added and the cells were incubated for another 1 h. Then the medium was removed and the cells were washed with PBS for three times. 4% paraformaldehyde (PFA) solution was added to fix the cells for 10 min, followed by staining of cell nucleus with DAPI (2 μg/mL) for 10 min. The coverslips were mounted on microscope slides with the addition of ProLong Gold antifade reagent and the prepared samples were stored in dark for imaging.

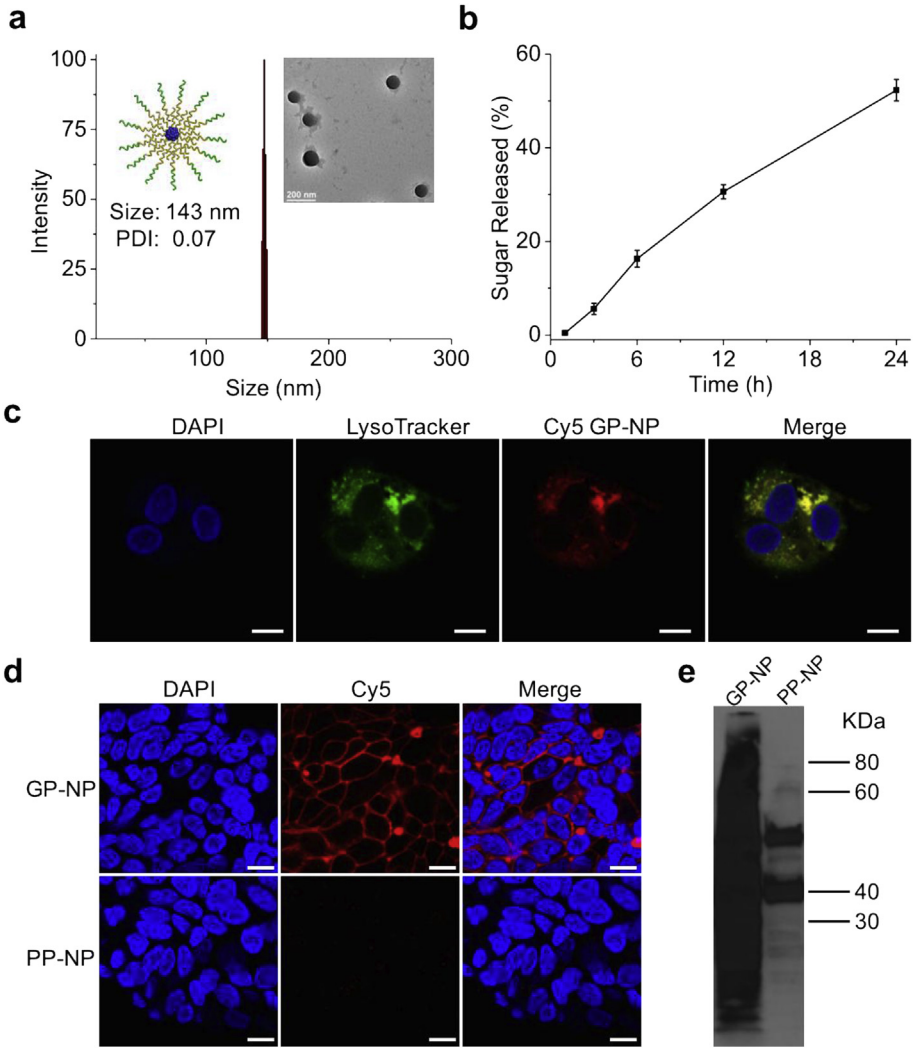

Fig. 1. (a) DLS analysis of GP-NP prepared from nanoprecipitation of GP and PEG-P(all). Inset: TEM characterization of GP-NP. (b) Release profile of sugar moieties from GP-NP in presence of esterase. Data were presented as average ± standard deviation, n = 3. (c) CLSM images of LS174T colon cancer cells after incubated with Cy5 GP-NP (5 μM) for 2 h. The cell nucleus was stained with DAPI. The Lysosomes/late endosomes were stained with LysoTracker Green DND-26 (Green). Scale bar: 10 μm. (d) CLSM images of LS174T colon cancer cells after incubated with GP-NP and PP-NP, respectively for 72 h and subsequently labeled with DBCO-Cy5 for 1 h. The cell nucleus was stained with DAPI. Scale bar: 10 μm. (e) Western blot analysis of LS174T cells after treated with GP-NP and PP-NP, respectively for 72 h. Azido-modified glycoproteins were converted to biotinylated ones prior to gel running and further analyses. (For interpretation of the references to colour in this figure legend, the reader is referred to the Web version of this article.)

2.6. Flow cytometry analysis

LS174T cells were seeded in a 24-well plate at a cell density of 10 k/well. GP-NP (25 μM in GP equivalent), PP-NP (25 μM in PP equivalent) or PBS was added and incubated with cells for 72 h. After removal of the medium and multiple washing steps, DBCO-Cy5 (25 μM) in opti-MEM was added and incubated with cells at 37 °C for 1 h. The medium was removed and cells were washed with PBS for three times. Then cells were lifted by incubation with trypsin solution (1 mL) at 37 °C for 3 min and transferred to test tubes with the addition of 4% PFA solution (0.5 mL). Ten thousand cells per sample were analyzed by flow cytometry and data analysis was performed on FCS Express software.

2.7. Western blot analysis of cells

LS174T cells were seeded onto cell culture flasks with a density of 1×10^6 cells per plate in 5 mL of medium. GP-NP (25 μM in GP equivalent), PP-NP (25 μM in PP equivalent) or PBS was added and incubated for three days. The cells were washed with PBS twice and harvested from the flasks with a cell scraper. Cells were pelleted by centrifugation at 1500 rpm for 5 min and resuspended in 200 μL of lysis buffer (1% SDS, 100 mM Tris·HCl, pH 7.4) containing one tablet of protease inhibitor (EDTA-free). The lysate was incubated at 4 °C for 30 min, followed by centrifugation at 3000 rcf for 10 min to remove insoluble cell debris. The total soluble protein concentration was determined by bicinchoninic acid (BCA) assay and adjusted to 1.5 mg/mL for all groups. Then 20 μL of the lysate was incubated with phosphine-PEG_3-biotin (2 μL, 5 mM in PBS) at 37 °C for 6 h. Loading buffer was added to each sample and samples were loaded onto 10% SDS-PAGE gel after heating at 95 °C for 5 min. After running the gel at 120 V for 105 min, protein bands were transferred to Hybond P membrane, followed by blocking of the membrane with 5% bovine serum albumin (BSA) in TBST (50 mM Tris.HCl, 150 mM NaCl, 0.1% Tween 20, pH 7.4) for 2 h. The membrane was then incubated with streptavidin-HRP (diluted 1:2000 in TBST) overnight at 4 °C, rinsed with TBST for three times, and developed by ECL Western Blotting Substrate.

2.8. In vivo and ex vivo fluorescence imaging

LS174T tumor models were established on 6 week-old female 01B74 athymic nude mice by subcutaneous injection of LS174T colon cancer cells (1.5 million) into both flanks. When the tumors grew to a size of ~6 mm, GP-NP (40 mg/kg in sugar equivalent) or PP-NP (same amount of NPs) or PBS was administered intravenously (i.v.) once daily for three days. 24 h after the last injection, DBCO-Cy5 (6 mg/kg) was i.v. injected. Nude mice were placed on the sample stage equipped with anesthesia input and output ports, and imaged by the Bruker Xtreme In-Vivo Fluorescence Imaging System at selected time points. The excitation filter was set at 630 nm and emission filter was set at 700 nm. Collected images were analyzed by the Bruker molecular imaging software. Major organs and tumors were dissected from mice at 6 h, 24 h or 48 h post injection of DBCO-Cy5. The ex vivo imaging was taken

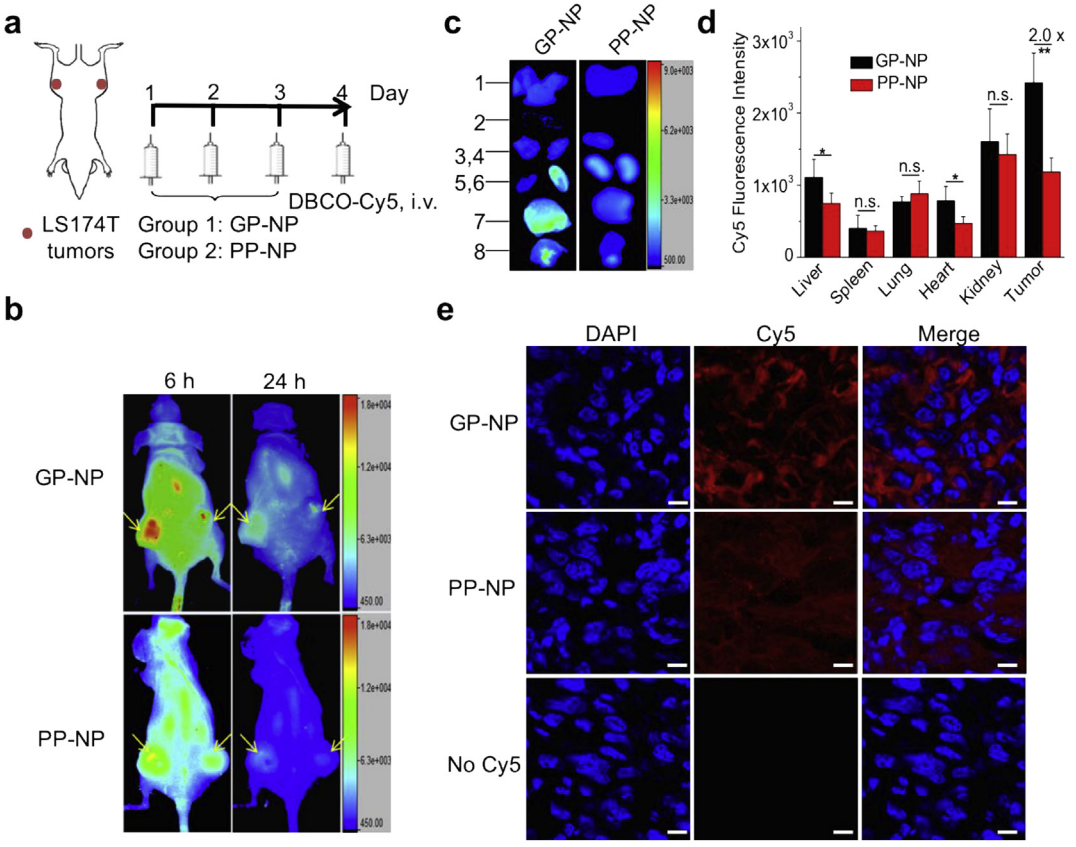

Fig. 2. *In vivo* labeling study of GP-NP and PP-NP. (a) Time frame of in vivo labeling study. Athymic nude mice bearing LS174T tumors on both flanks were i.v. injected with GP-NP (40 mg/kg in sugar equivalent) or PP-NP (same amount of NP) once daily for three days, and subsequently detected by DBCO-Cy5 (6 mg/kg). (b) *In vivo* whole body fluorescence imaging of mice pretreated with GP-NP (upper row) or PP-NP (lower row) at 6 and 24 h p.i. of DBCO-Cy5, respectively. Tumors were shown by yellow arrows. Scale unit: Counts per second. (c) *Ex vivo* fluorescence imaging of tumors and major organs (1-liver, 2-spleen, 3-lung, 4-heart, 5-kidney, 6-kidney, 7, 8-tumors). Scale unit: Counts per second. (d) Quantification of Cy5 FI of tumors and major organs from (c). Data were presented as average ± standard deviation, n = 4. Statistical significance analysis was performed by Two-Sample Unpaired Student's t-test; $0.05 < p$, $0.01 < *p \leq 0.05$ and $**p \leq 0.01$ were considered statistically non-significant, significant, and highly significant, respectively. (e) CLSM images of tumor sections from mice treated with GP-NP/DBCO-Cy5, PP-NP/DBCO-Cy5, and PBS, respectively. Cell nucleus was stained with DAPI (blue). Scale bar: 20 μm. The parameters for confocal imaging were kept the same for all samples. (For interpretation of the references to colour in this figure legend, the reader is referred to the Web version of this article.)

similarly using the Bruker Xtreme In-vivo Imaging System. Ex vivo images were quantified by measuring fluorescence intensity at selected ROIs. All values were expressed as means ± standard deviation.

For pharmacokinetics and biodistribution study of Cy5-labeled GP-NP, Cy5-labeled GP-NP was i.v. administered to tumor-bearing mice. Blood was collected at 1, 2, 4, 8, 12, and 24 h post injection of Cy5-labeled GP-NP, placed in a 96-well plate, and quantified for Cy5 fluorescence intensity using the Bruker Xtreme In-vivo Imaging System. In another parallel study, at 24 h or 48 h post injection of Cy5-labeled GP-NP, tumors and major organs were collected, homogenized, and quantified for Cy5 fluorescence intensity using the Bruker Xtreme In-vivo Imaging System.

2.9. Confocal imaging of tumor tissue

After ex vivo imaging, tumors were immediately frozen in O.C.T. compound. Tumor sections with a thickness of 6 μm were collected by cryostat (Leica CM3050S). DAPI in PBS (2 μg/mL) was added to the microscope slides to stain cell nucleus. After 10 min, DAPI solution was removed and the microscope slides were washed with PBS for three times. Coverslips were mounted on the microscope slides with the addition of ProLong Gold antifade reagent and the prepared samples were stored in dark for confocal imaging.

2.10. Synthesis of DBCO-hz-Dox

DBCO-NHS (40.2 mg, 0.1 mmol) was dissolved in anhydrous acetonitrile (1 mL), followed by addition of hydrazine (16.0 mg, 0.5 mmol). The mixture was stirred at room temperature for 30 h. The solvent was removed under reduced pressure and the residue was dissolved in anhydrous DMF (500 μL). Doxorubicin hydrochloride (58.0 mg, 0.1 mmol) in DMF (500 μL) was added, followed by addition of one drop of concentrated hydrochloric acid. The reaction mixture was stirred at 40 °C for 48 h. DBCO-hz-Dox was obtained via precipitation of the reaction mixture into diethyl ether and washed with diethyl ether for twice (overall yield: 70%). LRMS (ESI) *m/z*: exact mass calculated for $C_{46}H_{45}N_4O_{12}$ $[M+H]^+$ 845.3, found 845.6.

2.11. Release kinetics of DBCO-hz-Dox

DBCO-hz-Dox (1 mg) was dissolved in 1 mL of PBS (2% DMSO) with a pH value of 5.0 or 6.5 or 7.4, and incubated at 37 °C with gentle shaking. At selected time points (15 min, 30 min, 1 h, 2 h, 4 h, 6 h), 10 μL of DBCO-hz-Dox solution was injected into HPLC. Percentage of released Dox was determined by the standard curve of Dox.

2.12. MTT study of DBCO-hz-Dox and free Dox

In vitro cytotoxicity of DBCO-hz-Dox and free Dox was measured by

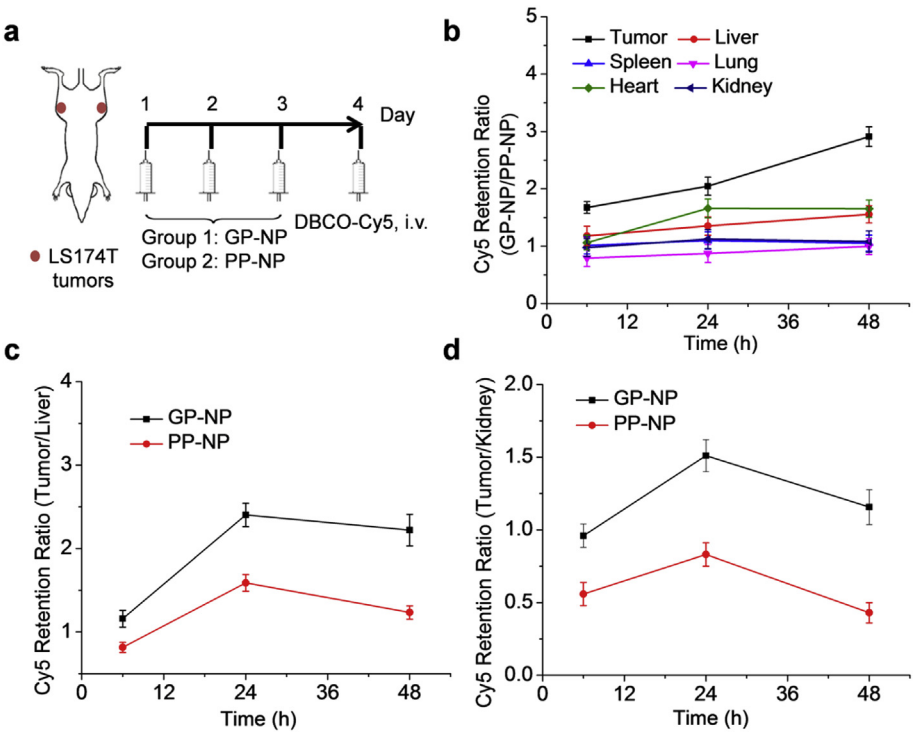

Fig. 3. GP-NP treatment improved the tumor retention of DBCO-Cy5. (a) Time axis of in vivo labeling study. Athymic nude mice bearing LS174T tumors on both flanks were i.v. injected with GP-NP (40 mg/kg in sugar equivalent) or PP-NP (same amount of NP) once daily for three days, and subsequently detected by DBCO-Cy5 (6 mg/kg). (b) Cy5 retention ratio of GP-NP treated mice to PP-NP treated mice in tumor and major organs at 6 h, 24 h, and 48 h p.i., respectively. Cy5 retention ratio of (c) tumor to liver and (d) tumor to kidney over time (6 h, 24 h, and 48 h p.i.) in mice treated with GP-NP (black line) and PP-NP (red line), respectively. Data were presented as average ± standard deviation, n = 3. (For interpretation of the references to colour in this figure legend, the reader is referred to the Web version of this article.)

MTT assay. LS174T colon cancer cells were seeded in a 96-well plate at an initial density of 4k cells/well, allowed to attach for 24 h, and treated with DBCO-hz-Dox or free Dox at various Dox concentrations at 37 °C for 48 h. Cells without drug treatment were used as control. The MTT assay was performed by following the standard procedure.

2.13. Antitumor efficacy study

LS174T tumor models were established on 6 week-old female 01B74 athymic nude mice by subcutaneous injection of LS174T colon cancer cells (1.5 million) into both flanks. When the tumors grew to a size of ~6 mm, mice were randomly divided into five groups (group 1: GP-NP/DBCO-hz-Dox; group 2: PP-NP/DBCO-hz-Dox; group 3: DBCO-hz-Dox; group 4: GP-NP; group 5: PBS; N = 3). For group 1 and group 4 mice, GP-NP (40 mg/kg in sugar equivalent) was i.v. injected once daily for three days. For group 2 and 3 mice, PP-NP (same amount of NPs) and PBS were i.v. injected, respectively once daily for three days. At 24 h post the last injection, DBCO-hz-Dox (10 mg/kg Dox equivalent) was i.v. injected into group 1, 2, and 3 mice. Group 4 and 5 mice were treated with PBS instead. At 48 h post injection of DBCO-hz-Dox, major organs and tumors were harvested. Tumors were cut into halves. Organs and half of the tumors were homogenized and lysed in lysis buffer (1% SDS, 100 mM Tris·HCl, pH 7.4). After the addition of acidified isopropanol, the mixture was vortexed and frozen overnight at −20 °C. After centrifugation, the supernatant was injected into HPLC for the quantification of retained Dox in tissues. Data were presented as %I.D./g. The other half of tumors were frozen with O.C.T. compound, and sectioned on cryostat (Leica CM3050S) with a thickness of 6 μm. Cell apoptosis in tumors was analyzed via terminal deoxynucleotidyl transferase dUTP nick end labeling (TUNEL) assay using in situ cell death detection kit (Roche Diagnostics GmbH, Mannheim, Germany). TUNEL staining was performed following the manufacture's manual. The tumor sections were imaged with the confocal laser scanning microscopy (LSM 700, Zeiss) at 20 × magnification. Cells under apoptosis were red fluorescent and all the nuclei were blue fluorescent.

2.14. Statistical analysis

The statistical analysis was performed by one-way analysis of variance (ANOVA) with post hoc Fisher's LSD test (OriginPro 8.5), and P-values < 0.05 were considered statistically significant. The results were deemed significant at $0.01 < {}^{*}P \leq 0.05$, highly significant at $0.001 < {}^{**}P \leq 0.01$, and extremely significant at ${}^{***}P \leq 0.001$.

3. Results and discussions

Hydroxyl-containing-substrate initiated ROP of *O*-carboxyanhydrides (OCAs) provides an efficient method to prepare biodegradable polyesters with controlled molecular weights (MWs), various functionalities, and tunable physicochemical properties [41]. Such substrate-polyester conjugates can be used to make polyester NPs with controlled release profiles [42,43]. As the exposure of the 1-OH of Ac_4ManAz is essential for its metabolic activity [31,32], we envisioned that using this 1–OH group to initiate ROP of OCAs to yield sugar-conjugated polyesters can not only achieve controlled sugar release profiles but also "preserve" cell labeling capability until the azido-sugar is released from the polymeric structure. Ac_3ManAzOH was obtained via site-specific deprotection of Ac_4ManAz (Scheme 1a, Fig. S1). GP(all)s with well controlled MWs and narrow polydispersities were prepared via Ac_3ManAzOH initiated ROP of all-OCA using 4-dimethylaminopyridine (DMAP) as the catalyst (Table S1 and Fig. S4a). We selected GP$(all)_{20}$, a 20-mer GP, throughout this study due to its highest sugar contents among all GP(all)s synthesized. Pyrene-P$(all)_{20}$ (PP) and PEG_{5k}-P$(all)_{20}$ (PEG-P(all)) were similarly prepared using 1-pyrenebutanol and methoxy polyethylene glycol (mPEG, MW = 5k Da) as the initiator, respectively (Table S2, Fig. S6).

We then prepared NPs via nanoprecipitation of GP (or PP) with PEG-P(all) [10]. The resulting GP-NP had an average diameter of 143 nm and a narrow PDI of 0.07, as determined by dynamic light scattering (DLS, Fig. 1a). TEM showed a smaller diameter, at around 113 nm (Inset, Fig. 1a). PP-NP with a similar diameter was confirmed by DLS and TEM analysis (Fig. S7). Both GP- and PP-NP showed remarkable stability in 50% human serum, evidenced by the negligible size changes over 9 days (Fig. S8). To understand the sugar release

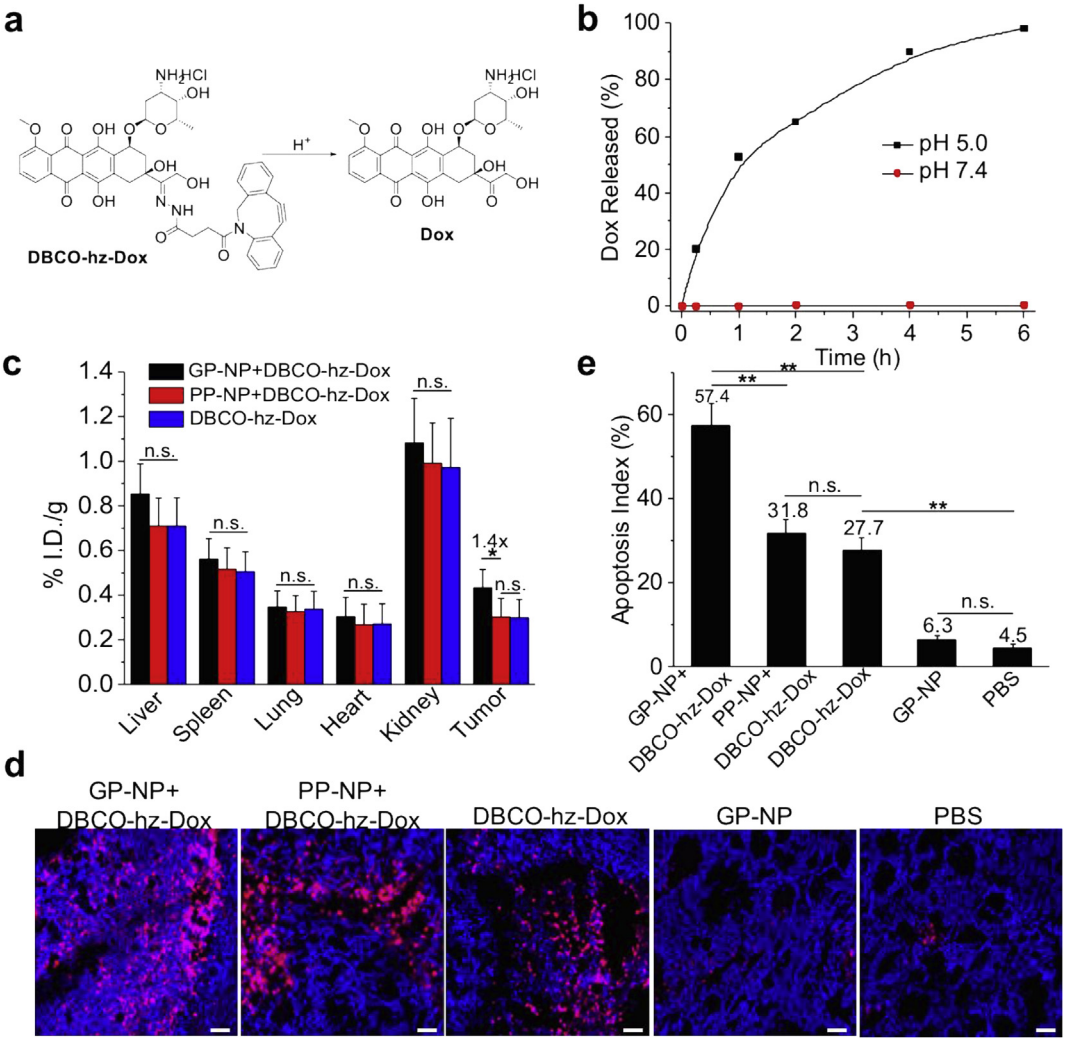

Fig. 4. (a) Structure of pH-responsive DBCO-hz-Dox. (b) Release kinetic profiles of DBCO-hz-Dox at pH 5.0 and 7.4, respectively. (c-e) GP-NP (40 mg/kg in sugar equivalent) or PP-NP was i.v. injected once daily for three days (Day 0–2), followed by i.v. injection of DBCO-hz-Dox (10 mg/kg in Dox equivalent) on Day 3. Mice were sacrificed and analyzed on Day 5. (c) Retained Dox in tumors and major organs from mice treated with GP-NP + DBCO-hz-Dox, PP-NP + DBCO-hz-Dox, and DBCO-hz-Dox, respectively at 48 h post injection of DBCO-hz-Dox. Dox was extracted from acidified tissue lysates and quantified using HPLC. (d) Representative TUNEL staining sections of harvested LS174T tumors after different treatments. Scale bar: 50 μm. (e) Quantification of TUNEL stains via ImageJ. The apoptosis index was determined as the ratio of apoptotic cell number (TUNEL, red) to the total cell number (DAPI, blue). 20 tissue sections were counted per tumor, n = 6. (For interpretation of the references to colour in this figure legend, the reader is referred to the Web version of this article.)

kinetics of GP-NP, we conjugated DBCO-Cy5 to GP first to yield Cy5-labeled GP (Cy5 GP) and then prepared Cy5-labeled GP-NP (Cy5 GP-NP) via nanoprecipitation of Cy5 GP with PEG-P(all). We found that ~50% of sugar moieties were released from GP-NP in 24 h in the presence of esterase (Fig. 1b), showing a controlled release rate on the same order of magnitude as the rate of metabolic labeling process of unnatural sugars [31,44]. CLSM images of LS174T cells incubated with Cy5 GP-NP for 2 h showed the overlay of Cy5 signal with LysoTracker Green signal (Fig. 1c), which confirmed that GP-NP entered late endosomes and might release sugar moities there for subsequent metabolic cell labeling.

We next evaluated GP-NP with covalent attachment of azido-sugars for cell labeling. LS174T cells were incubated with GP-NP or PP-NP for 72 h and further incubated with DBCO-Cy5 for 1 h. Confocal images of LS174T cells treated with GP-NP showed clear and uniform Cy5 fluorescence on the cell surface (Fig. 1d, upper panel) in comparison to the negligible Cy5 fluorescence observed in cells treated with PP-NP (Fig. 1d, lower panel), indicating the successful labeling of LS174T cells with azido groups by GP-NP. Flow cytometry analysis also showed the significantly enhanced Cy5 fluorescence intensity (FI) of LS174T cells treated with GP-NP than cells treated with PP-NP (Fig. S9). To confirm that the azido groups were expressed in the form of glycoproteins, Western blot analysis of LS174T cells with GP-NP or PP-NP treatment was conducted. By incubating with biotin-PEG_4-phosphine, azido-modified glycoproteins were converted to biotinylated ones and thus could be easily detected. LS174T cells treated with GP-NP showed a series of protein bands, while cells treated with PP-NP only showed significantly less protein signals (Fig. 1e). This experiment substantiated the successful metabolic incorporation of azido groups into cell-surface glycoproteins.

After demonstrating in vitro labeling property of GP-NP, we next investigated its cancer labeling capability in vivo and the resulting Click reaction-mediated targeting effect. We first studied the pharmacokinetics of GP-NP, which showed that the majority of GP-NP was cleared from bloodstream within 24 h (Fig. S10). GP-NP (or PP-NP) was then administered intravenously (i.v.) to athymic nude mice bearing subcutaneous LS174T tumors once daily for three days. At 24 h post injection (p.i.), DBCO-Cy5 was i.v. injected and its biodistribution was monitored via in vivo fluorescence imaging (Fig. 2a). At 6 h and 24 h p.i., a clear fluorescence contrast between tumors and the rest of the

body was observed in mice pretreated with GP-NP, while tumors in PP-NP group showed similar Cy5 retention to the rest of the body, indicating the enhanced tumor retention of DBCO-Cy5 by Click reaction in mice pretreated with GP-NP (Fig. 2b). Ex vivo imaging of tumors in GP-NP group showed a 2.05-fold Cy5 FI of the PP-NP group at 24 h p.i. of DBCO-Cy5 (Fig. 2c and d). Confocal images of tumor sections from GP-NP group also showed much stronger Cy5 FI than PP-NP group (Fig. 2e).

To understand the enhanced tumor retention of captured DBCO-Cy5 via Click reaction, we analyzed the biodistribution of DBCO-Cy5 over time in mice pretreated with GP-NP and PP-NP, respectively. At selected time points (6 h, 24 h, and 48 h p.i. of DBCO-Cy5), tumors and major organs were harvested for ex vivo imaging (Fig. 3a). GP-NP group showed much better tumor retention of DBCO-Cy5 over time compared to PP-NP group, with the Cy5 retention ratio in tumor increased from 1.68 at 6 h p.i. to 2.05 at 24 h p.i. to 2.91 at 48 h p.i.. (Fig. 3b, black line). The increasing tumor retention ratio over time suggests that DBCO-Cy5 was well retained by the expressed azido groups in the tumor area of GP-NP pretreated mice. Significantly smaller Cy5 retention ratio of GP-NP group to PP-NP group in liver, spleen, and heart was observed at 48 h p.i. (Fig. 3b, Fig. S11). The increased tumor-to-liver and tumor-to kidney ratios of Cy5 FI at 24 h and 48 h p.i. also testified the better tumor retention of DBCO-Cy5 in GP-NP group than in PP-NP group (Fig. 3c and d). These experiments demonstrated that GP-NP mediated metabolic labeling of tumor cells with azido groups can result in enhanced tumor retention of DBCO-Cy5 via Click reaction. While GP-NP also showed accumulation in healthy tissues including liver and spleen (Fig. S12), the sugar metabolism rate of cancer cells is generally much higher than normal cells [31]. As a combinatory result of the EPR effect and higher metabolism rate of cancer cells than normal cells, GP-NP could relatively better label tumor cells with azido groups, while showing less labeling in other tissues.

After demonstrating that GP-NP pretreatment could significantly enhance the tumor retention of DBCO-Cy5 via Click reaction, we next investigated whether GP-NP pretreatment would improve the tumor accumulation and anticancer efficacy of small molecule DBCO-drug conjugates. DBCO-doxorubicin conjugate with a pH-responsive hydrazone linker (DBCO-hz-Dox) was first synthesized (Fig. 4a). DBCO-hz-Dox showed good stability at pH 7.4 and slow degradation at pH 6.5 (Fig. S13), while releasing Dox rapidly at pH 5.0 (Fig. 4b and Fig. S14), suggesting that Dox may be subject to faster release in acidic cellular organelles, such as endosomes. In vitro anticancer efficacy of DBCO-hz-Dox against LS174T cells was studied via MTT assay, which showed an IC_{50} value of 0.54 μM (Fig. S15). In an acute antitumor efficacy study, athymic nude mice bearing LS174T tumors were pretreated with GP-NP or PP-NP once daily for three days, and i.v. injected with DBCO-hz-Dox. At 48 h p.i., tumors were harvested and analyzed for drug retention and cell apoptosis. GP-NP pretreatment improved the tumor accumulation of DBCO-hz-Dox by 40% (Fig. 4c) and resulted in a much higher apoptosis index (57.4 ± 5.1%) compared to PP-NP pretreatment (31.8 ± 3.2%) (Fig. 4d and e). Tumors treated with DBCO-hz-Dox alone showed comparable apoptosis (27.7 ± 2.8%) to tumors treated with PP-NP + DBCO-hz-Dox (31.8 ± 3.2%) (Fig. 4e), which further testified the importance of azido-sugars in tumor labeling. As negative controls, tumors treated with GP-NP or PBS showed much lower apoptosis index, with an apoptosis index of 6.3 ± 1.0% and 4.5 ± 0.9%, respectively (Fig. 4e).

4. Conclusion

In this paper, we report a new method to synthesize azido-sugar conjugated glycopolyesters via azido-sugar initiated polymerization of OCAs and further prepare NPs with narrow size distribution, excellent stability, and controlled sugar release. We demonstrated that GP-NP mediated azido-labeling of tumor cells could significantly improve the retention of DBCO-Cy5 and DBCO-drug conjugate, with a much slower tumor clearance rate over time. Also, GP-NP labeling showed limited effect on the distribution and retention of drugs in other non-cancerous tissues. Together, the reduced dose and side effects are anticipated via the use of this two-step targeted chemotherapy for cancer treatment. This reported GP-NP, with a typical nanoscale size and surface PEG-coating, coupled with DBCO-drug, may provide a new avenue for cancer targeting. The administration of biocompatible GP-NP, as the first step, enables manual introduction of chemical tags to tumor cell membranes. DBCO-drugs can then be targeted to tumor cells via efficient Click chemistry, potentially improving antitumor efficacy while reducing side effects. Our approach does not rely on endogenous protein receptors for targeting, so it is also applicable to various types of tumors lacking known targetable receptors, such as triple negative breast cancers. The biocompatibility and simplicity of GP-NP, and facile DBCO modification of various clinical drugs, can be easily applied to clinical chemotherapy and radiation therapy. Future work that can improve the tumor-labeling selectivity of azido-sugar materials will further facilitate the clinical translation of this two-step cancer targeting strategy.

Author contributions

The manuscript was written through contributions of all authors. All authors have given approval to the final version of the manuscript. The authors declare no competing financial interest.

Acknowledgment

This work is supported by NIH (Director's New Innovator Award 1DP2OD007246) and NSF (DMR 1309525). H.W. gratefully acknowledge the support from HHMI International Student Research Fellowship. We acknowledge the useful discussions with Prof. David J. Mooney at Harvard University.

Appendix A. Supplementary data

Supplementary data to this article can be found online at https://doi.org/10.1016/j.biomaterials.2019.119305.

References

[1] H. Maeda, SMANCS and polymer-conjugated macromolecular drugs: Advantages in cancer chemotherapy, Adv. Drug Deliv. Rev. 46 (1) (2001) 169–185.
[2] A.J. Wood, D.C. Ihde, Chemotherapy of lung cancer, N. Engl. J. Med. 327 (20) (1992) 1434–1441.
[3] S. Banerjee, Y. Li, Z. Wang, F.H. Sarkar, Multi-targeted therapy of cancer by genistein, Cancer Lett. 269 (2) (2008) 226–242.
[4] C. Sawyers, Targeted cancer therapy, Nature 432 (7015) (2004) 294–297.
[5] T.A. ElBayoumi, V.P. Torchilin, Tumor-targeted nanomedicines: Enhanced antitumor efficacy in vivo of doxorubicin-loaded, long-circulating liposomes modified with cancer-specific monoclonal antibody, Clin. Cancer Res. 15 (6) (2009) 1973–1980.
[6] Y. Liu, H. Miyoshi, M. Nakamura, Nanomedicine for drug delivery and imaging: A promising avenue for cancer therapy and diagnosis using targeted functional nanoparticles, Int. J. Cancer 120 (12) (2007) 2527–2537.
[7] R. Duncan, Polymer conjugates as anticancer nanomedicines, Nat. Rev. Canc. 6 (9) (2006) 688–701.
[8] D.B. Kirpotin, D.C. Drummond, Y. Shao, M.R. Shalaby, K. Hong, U.B. Nielsen, J.D. Marks, C.C. Benz, J.W. Park, Antibody targeting of long-circulating lipidic nanoparticles does not increase tumor localization but does increase internalization in animal models, Cancer Res. 66 (13) (2006) 6732–6740.
[9] O.C. Farokhzad, J. Cheng, B.A. Teply, I. Sherifi, S. Jon, P.W. Kantoff, J.P. Richie, R. Langer, Targeted nanoparticle-aptamer bioconjugates for cancer chemotherapy in vivo, Proc. Natl. Acad. Sci. Unit. States Am. 103 (16) (2006) 6315–6320.
[10] J. Cheng, B.A. Teply, I. Sherifi, J. Sung, G. Luther, F.X. Gu, E. Levy-Nissenbaum, A.F. Radovic-Moreno, R. Langer, O.C. Farokhzad, Formulation of functionalized PLGA-PEG nanoparticles for in vivo targeted drug delivery, Biomaterials 28 (5) (2007) 869–876.
[11] K. Maruyama, N. Takahashi, T. Tagawa, K. Nagaike, M. Iwatsuru, Immunoliposomes bearing polyethyleneglycol-coupled Fab′ fragment show prolonged circulation time and high extravasation into targeted solid tumors in vivo, FEBS Lett. 413 (1) (1997) 177–180.

[12] D.K. Kim, J. Dobson, Nanomedicine for targeted drug delivery, J. Mater. Chem. 19 (35) (2009) 6294–6307.
[13] F. Danhier, O. Feron, V. Préat, To exploit the tumor microenvironment: Passive and active tumor targeting of nanocarriers for anti-cancer drug delivery, J. Control. Release 148 (2) (2010) 135–146.
[14] O.C. Farokhzad, J. Cheng, B.A. Teply, I. Sherifi, S. Jon, P.W. Kantoff, J.P. Richie, R. Langer, Targeted nanoparticle-aptamer bioconjugates for cancer chemotherapy in vivo, Proc. Natl. Acad. Sci. Unit. States Am. 103 (16) (2006) 6315–6320.
[15] E. Pérez-Herrero, A. Fernández-Medarde, Advanced targeted therapies in cancer: Drug nanocarriers, the future of chemotherapy, Eur. J. Pharm. Biopharm. 93 (2015) 52–79.
[16] T. Lammers, F. Kiessling, W.E. Hennink, G. Storm, Drug targeting to tumors: Principles, pitfalls and (pre-) clinical progress, J. Control. Release 161 (2) (2012) 175–187.
[17] J.A. Codelli, J.M. Baskin, N.J. Agard, C.R. Bertozzi, Second-generation difluorinated cyclooctynes for copper-free click chemistry, J. Am. Chem. Soc. 130 (34) (2008) 11486–11493.
[18] H. Koo, S. Lee, J.H. Na, S.H. Kim, S.K. Hahn, K. Choi, I.C. Kwon, S.Y. Jeong, K. Kim, Bioorthogonal copper-free click chemistry in vivo for tumor-targeted delivery of nanoparticles, Angew. Chem. Int. Ed. 51 (47) (2012) 11836–11840.
[19] H.C. Kolb, K.B. Sharpless, The growing impact of click chemistry on drug discovery, Drug Discov. Today 8 (24) (2003) 1128–1137.
[20] J.E. Moses, A.D. Moorhouse, The growing applications of click chemistry, Chem. Soc. Rev. 36 (8) (2007) 1249–1262.
[21] K. Nwe, M.W. Brechbiel, Growing applications of “click chemistry” for bioconjugation in contemporary biomedical research, Cancer Biother. Radiopharm. 24 (3) (2009) 289–302.
[22] C.D. Hein, X.-M. Liu, D. Wang, Click chemistry, a powerful tool for pharmaceutical sciences, Pharm. Res. 25 (10) (2008) 2216–2230.
[23] J.A. Prescher, D.H. Dube, C.R. Bertozzi, Chemical remodelling of cell surfaces in living animals, Nature 430 (7002) (2004) 873–877.
[24] P.V. Chang, J.A. Prescher, E.M. Sletten, J.M. Baskin, I.A. Miller, N.J. Agard, A. Lo, C.R. Bertozzi, Copper-free click chemistry in living animals, Proc. Natl. Acad. Sci. Unit. States Am. 107 (5) (2010) 1821–1826.
[25] S.J. Luchansky, H.C. Hang, E. Saxon, J.R. Grunwell, C. Yu, D.H. Dube, C.R. Bertozzi, Constructing azide-labeled cell surfaces using polysaccharide biosynthetic pathways, in: C.L. Yuan, T.L. Reiko (Eds.), Methods in Enzymology, vol. 362, Academic Press, 2003, pp. 249–272.
[26] P.V. Chang, X. Chen, C. Smyrniotis, A. Xenakis, T. Hu, C.R. Bertozzi, P. Wu, Metabolic labeling of sialic acids in living animals with alkynyl sugars, Angew. Chem. Int. Ed. 48 (22) (2009) 4030–4033.
[27] S.T. Laughlin, N.J. Agard, J.M. Baskin, I.S. Carrico, P.V. Chang, A.S. Ganguli, M.J. Hangauer, A. Lo, J.A. Prescher, C.R. Bertozzi, Metabolic labeling of glycans with azido sugars for visualization and glycoproteomics, Methods Enzymol. 415 (2006) 230–250.
[28] L. Yang, J.O. Nyalwidhe, S. Guo, R.R. Drake, O.J. Semmes, Targeted identification of metastasis-associated cell-surface sialoglycoproteins in prostate cancer, Mol. Cell. Proteom. 10 (6) (2011) 007294 M110.
[29] K. Fukase, K. Tanaka, Bio-imaging and cancer targeting with glycoproteins and N-glycans, Curr. Opin. Chem. Biol. 16 (5) (2012) 614–621.
[30] K.-C. Tsai, J.-W. Jian, E.-W. Yang, P.-C. Hsu, H.-P. Peng, C.-T. Chen, J.-B. Chen, J.-Y. Chang, W.-L. Hsu, A.-S. Yang, Prediction of carbohydrate binding sites on protein surfaces with 3-dimensional probability density distributions of interacting atoms, PLoS One 7 (7) (2012) e40846.
[31] H. Wang, R. Wang, K. Cai, H. He, Y. Liu, J. Yen, Z. Wang, M. Xu, Y. Sun, X. Zhou, Selective in vivo metabolic cell-labeling-mediated cancer targeting, Nat. Chem. Biol. 13 (4) (2017) 415–424.
[32] P.V. Chang, D.H. Dube, E.M. Sletten, C.R. Bertozzi, A strategy for the selective imaging of glycans using caged metabolic precursors, J. Am. Chem. Soc. 132 (28) (2010) 9516–9518.
[33] R. Xie, S. Hong, L. Feng, J. Rong, X. Chen, Cell-selective metabolic glycan labeling based on ligand-targeted liposomes, J. Am. Chem. Soc. 134 (24) (2012) 9914–9917.
[34] R. Xie, L. Dong, R. Huang, S. Hong, R. Lei, X. Chen, Targeted imaging and proteomic analysis of tumor-associated glycans in living animals, Angew. Chem. 126 (51) (2014) 14306–14310.
[35] H. Wang, M. Gauthier, J.R. Kelly, R.J. Miller, M. Xu, W.D. O'Brien, J. Cheng, Targeted ultrasound-assisted cancer-selective chemical labeling and subsequent cancer imaging using click chemistry, Angew. Chem. 128 (18) (2016) 5542–5546.
[36] R. Xie, S. Hong, X. Chen, Cell-selective metabolic labeling of biomolecules with bioorthogonal functionalities, Curr. Opin. Chem. Biol. 17 (5) (2013) 747–752.
[37] H. Maeda, J. Wu, T. Sawa, Y. Matsumura, K. Hori, Tumor vascular permeability and the EPR effect in macromolecular therapeutics: A review, J. Control. Release 65 (1) (2000) 271–284.
[38] J. Fang, H. Nakamura, H. Maeda, The EPR effect: Unique features of tumor blood vessels for drug delivery, factors involved, and limitations and augmentation of the effect, Adv. Drug Deliv. Rev. 63 (3) (2011) 136–151.
[39] L. Tang, X. Yang, Q. Yin, K. Cai, H. Wang, I. Chaudhury, C. Yao, Q. Zhou, M. Kwon, J.A. Hartman, I. Dobrucki, L. Dobrucki, L. Borst, S. Lezmi, W. Helferich, A. Ferguson, T. Fan, J. Cheng, Investigating the optimal size of anticancer nanomedicine, Proc. Natl. Acad. Sci. Unit. States Am. 111 (43) (2014) 15344–15349.
[40] S. Lee, H. Koo, J.H. Na, S.J. Han, H.S. Min, S.J. Lee, S.H. Kim, S.H. Yun, S.Y. Jeong, I.C. Kwon, K. Choi, K. Kim, Chemical tumor-targeting of nanoparticles based on metabolic glycoengineering and click chemistry, ACS Nano 8 (3) (2014) 2048–2063.
[41] H. Wang, L. Tang, C. Tu, Z. Song, Q. Yin, L. Yin, Z. Zhang, J. Cheng, Redox-responsive, core-cross-linked micelles capable of on-demand, concurrent drug release and structure disassembly, Biomacromolecules 14 (10) (2013) 3706–3712.
[42] R. Tong, J. Cheng, Ring-opening polymerization-mediated controlled formulation of Polylactide – Drug nanoparticles, J. Am. Chem. Soc. 131 (13) (2009) 4744–4754.
[43] R. Tong, J. Cheng, Ring-opening polymerization-mediated controlled formulation of Polylactide – drug nanoparticles, J. Am. Chem. Soc. 131 (13) (2009) 4744–4754.
[44] K.J. Yarema, L.K. Mahal, R.E. Bruehl, E.C. Rodriguez, C.R. Bertozzi, Metabolic delivery of ketone groups to sialic acid residues application to cell surface glycoform engineering, J. Biol. Chem. 273 (47) (1998) 31168–31179.